PAPER

Emission and capture characteristics of electron trap (E_{emi} = 0.8 eV) in Si-doped β-Ga$_2$O$_3$ epilayer

To cite this article: Haolan Qu *et al* 2023 *Semicond. Sci. Technol.* **38** 015001

View the article online for updates and enhancements.

Emission and capture characteristics of electron trap (E_{emi} = 0.8 eV) in Si-doped β-Ga$_2$O$_3$ epilayer

Haolan Qu[1,2,3] ⓘ **, Jiaxiang Chen**[1,2,3] ⓘ **, Yu Zhang**[1,2,3] ⓘ **, Jin Sui**[1,2,3]**, Yitian Gu**[1,2,3]**,
Yuxin Deng**[4]**, Danni Su**[4]**, Ruohan Zhang**[1,5]**, Xing Lu**[4] ⓘ **and Xinbo Zou**[1,5,*] ⓘ

[1] School of Information Science and Technology, ShanghaiTech University, Shanghai 201210,
People's Republic of China
[2] Shanghai Institute of Microsystem and Information Technology, Chinese Academy of Sciences,
Shanghai 200050, People's Republic of China
[3] School of Microelectronics, University of Chinese Academy of Sciences, Beijing 100049,
People's Republic of China
[4] School of Electronics and Information Technology, Sun Yat-sen University, Guangzhou 510275,
People's Republic of China
[5] Shanghai Engineering Research Center of Energy Efficient and Custom AI IC, Shanghai 200031,
People's Republic of China

E-mail: zouxb@shanghaitech.edu.cn

CrossMark

Abstract

By deep level transient spectroscopy (DLTS), emission and capture behaviors have been
explicitly investigated for a single electron trap in a Si-doped β-Ga$_2$O$_3$ epilayer. Trap
characteristics including activation energy for emission (E_{emi} = 0.8 eV), capture cross-section
of 6.40×10^{-15} cm^2 and lambda-corrected trap concentration (N_{Ta}) of 2.48×10^{13} cm^{-3} were
revealed, together with non-emission region width (λ = 267.78 nm). By isothermal DLTS, in
addition to the impact of temperature, electric-field-enhanced trap emission kinetics were
studied. When a relatively low electric field was applied ($E \leqslant 1.81 \times 10^5$ V cm^{-1} at 330 K),
emission kinetics of the trap was modeled to comply with phonon-assisted tunneling, whereas
the emission process was regarded to be dominated by direct tunneling for a relatively high
electric field ($E \geqslant 1.81 \times 10^5$ V cm^{-1} at 330 K). A thermal-enhanced capture process has also
been disclosed and quantitatively studied, where a capture barrier energy of 0.15 eV was
extracted.

Supplementary material for this article is available online

Keywords: β-Ga$_2$O$_3$, epilayer, deep level transient spectroscopy, trap, emission, capture

(Some figures may appear in colour only in the online journal)

1. Introduction

β-Ga$_2$O$_3$ has been attracting extensive research interest for
power conversion applications, owing to its ultrawide bandgap
(4.9 eV), high critical electric field of 8 MV cm^{-1}, and excel-
lent thermal stability [1–3]. In addition to β-Ga$_2$O$_3$ devices
based on bulk semiconducting materials [4, 5], there have been
ample efforts devoted to development of β-Ga$_2$O$_3$ epitaxial
layers and devices [6–10]. High-quality β-Ga$_2$O$_3$ homogen-
eous epilayers with low effective donor concentration have
been grown and demonstrated by hydride vapor phase epitaxy

---

* Author to whom any correspondence should be addressed.

(HVPE) [10]. Using a 20 μm -thick epitaxial layer, Yang *et al* reported a β-Ga$_2$O$_3$ field-plated Schottky rectifier with a breakdown voltage of 2300 V [11]. Polyakov *et al* reported that trap concentration in a β-Ga$_2$O$_3$ epilayer could be substantially reduced, compared to trap concentration in the β-Ga$_2$O$_3$ substrate [12].

Deep level traps in β-Ga$_2$O$_3$ have often been linked to threshold voltage (V_{th}) instability and on-resistance (R_{on}) increase in Ga$_2$O$_3$ devices, thus it is demanding to gain a comprehensive understanding of trap properties [13]. Deep level traps with activation energy for emission (E_{emi}) from 0.6 eV to 1.0 eV have been reported in devices using β-Ga$_2$O$_3$ epilayers [6, 12, 14, 15]. Among all the deep level traps, electron trap with its E_{emi} of 0.8 eV has been identified by a number of methods including thermally stimulated current spectroscopy [15], deep level transient spectroscopy (DLTS) [6, 12] and optical DLTS [14]. In a 20 μm Si-doped β-Ga$_2$O$_3$ epilayer grown by HVPE, the trap concentration of an electron trap (E_{emi} = 0.75 eV) was found to increase after proton irradiation [12]. Temperature-dependent (T-dependent) emission time constant of trap (E_{emi} = 0.77 eV) has also been reported for an undoped 100 nm β-Ga$_2$O$_3$ epilayer grown by plasma-assisted molecular beam epitaxy [13].

Despite the steady progress towards understanding deep level trap (E_{emi} = 0.8 eV) in homoepitaxial grown β-Ga$_2$O$_3$ layer, there are still some issues to be addressed before achieving a thorough understanding of this particular trap level in the β-Ga$_2$O$_3$ epilayer. (a) Emission behaviors of electron traps in β-Ga$_2$O$_3$ play an important role in investigating device properties, e.g. compensation of conductivity, or recombination of nonequilibrium charge carriers [16]. There have been some reports on emission kinetics of traps in an undoped β-Ga$_2$O$_3$ bulk crystal [17]; however, de-trapping behaviors of deep level trap (E_{emi} = 0.8 eV) as a function of electric field are still unknown for a Si-doped β-Ga$_2$O$_3$ epilayer. (b) Both carrier emission rates and capture rates are highly dependent on electron capture barrier energy (E_{cap}) [18]. Meanwhile, without knowing the capture barrier energy, accurate determination of binding energy ($E_{binding}$) which reveals the depth of the trap with respect to the conduction band minimum would not be possible [19]. There has been few study on the capture barrier of a proton-irradiated β-Ga$_2$O$_3$ layer [12]. However, an insight into the E_{cap} and the $E_{binding}$ of deep level in a pristine Si-doped β-Ga$_2$O$_3$ epilayer are currently unavailable.

In this paper, emission and capture characteristics of electron trap (E_{emi} = 0.8 eV) in Si-doped β-Ga$_2$O$_3$ homogeneous epilayer have been investigated. Thermally-enhanced emission process has been explicitly analyzed with emission time constants. Electric-field-enhanced emission mechanisms of the trap were studied by isothermal DLTS measurements. By varying filling pulse width, the capture process of the trap was revealed, and the E_{cap} was extracted based on the amplitude of capacitance transient signal as well. The physical insight on the emission and capture process of the trap paves a solid path for a thorough understanding of the trap properties in β-Ga$_2$O$_3$ epilayer and interpretation of the electrical performance instability of β-Ga$_2$O$_3$ based power devices.

2. Device and electrical characteristics

Figure 1(a) shows the schematic cross section of the vertical β-Ga$_2$O$_3$ Schottky barrier diode (SBD) with homogeneous epilayer. The 11 μm Si-doped β-Ga$_2$O$_3$ epilayer was grown on the Sn-doped β-Ga$_2$O$_3$ substrate by HVPE, and the β-Ga$_2$O$_3$ substrate was grown by edge-defined film-fed growth. For β-Ga$_2$O$_3$ SBD fabrication, Ti/Al/Ni/Au metal stack was evaporated on the backside of the wafer to form ohmic contact. Finally, Ni/Au was deposited on the epilayer to obtain Schottky contact.

Figure 1(b) illustrates typical *I–V* characteristics of a fabricated β-Ga$_2$O$_3$ SBD (anode diameter = 400 μm). Threshold voltage (V_{th}) was determined to be 0.78 V, at a current density of 1 A cm^{-2} at room temperature. Reduced V_{th} from 0.92 V to 0.72 V displayed in figure 1(c) can be observed with rising temperature from 200 K to 350 K. Figure 1(d) depicts the *C–V* results of the SBD with a measurement frequency of 1 MHz. The built-in voltage (V_{bi}) and corresponding Schottky barrier height (Φ_B) can be extracted from *C–V* characteristics by the following equations [20, 21]:

$$\frac{1}{C^2} = \frac{2}{\varepsilon_r \varepsilon_0 q A^2 N_s} \left(V + V_{bi} - \frac{kT}{q} \right) \tag{1}$$

$$q\Phi_B = qV_{bi} + E_C - E_F = qV_{bi} - kT\ln\left(\frac{N_s}{N_C}\right) \tag{2}$$

where ε_r and ε_0 are relative and vacuum permittivity, respectively, q is the elementary charge, A is the anode area, k is the Boltzmann constant, and N_C is the effective density of states in the conduction band. Schottky barrier height (Φ_B), the built-in voltage (V_{bi}), and $E_C - E_F$ as a function of temperature are plotted in figure 1(e). As temperature increases from 200 K to 350 K, $q\Phi_B$ and qV_{bi} decrease slightly from 1.19 eV to 1.15 eV and from 1.11 eV to 0.98 eV respectively, which matches well with the reduced V_{th} at higher temperature. The net donor concentration of the epilayer, N_s of 2 × 10^{16} cm^{-3} can also be extracted from the *C–V* characteristics, as shown in the inset of figure 1(d).

3. Trap characteristics

DLTS measurement was performed to identify the existence and activation energy of trap in the β-Ga$_2$O$_3$ SBD with homogeneous epilayer. The DLTS measurements were conducted with a reverse bias $U_R = -20$ V and a filling pulse $U_P = -0.5$ V. Filling pulse width t_P and measurement period T_W were set to 0.8 s and 9 s, respectively. As shown in figure 2(a), temperature-scanning DLTS signal spectra revealed one majority carrier (electron) trap, named as E1 in this study. Figure 2(b) displays the Arrhenius plot of electron trap E1 obtained from DLTS spectra [22]. From Arrhenius analysis, an activation energy for emission (E_{emi}) of 0.80 eV, and capture cross section (σ_n) of 6.40 × 10^{-15} cm^2 could be extracted. Meanwhile, the depletion region width with U_R (w_R) was calculated to be 1.06 μm when $U_R = -20$ V, which

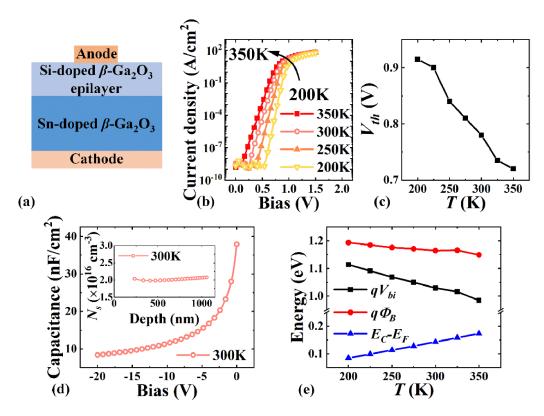**Figure 1.** (a) Schematic cross section of the vertical β-Ga$_2$O$_3$ Schottky barrier diode (SBD) with homogeneous epilayer. (b) Forward current–voltage (I–V) characteristics in logarithmic scale from 200 K to 350 K. (c) V_{th} extracted from forward I–V characteristics from 200 K to 350 K. (d) Capacitance–voltage (C–V) characteristics at 1 MHz. Inset: the net donor concentration (N_s) extracted from C–V characteristics at 300 K. (e) T-dependent Schottky barrier height (Φ_B), built-in voltage (V_{bi}) and the energy difference between Femi level (E_F) and conduction band minimum (E_C).
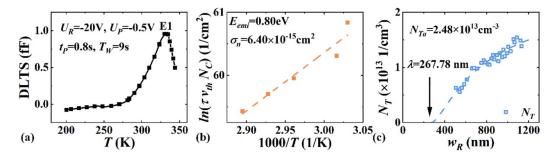

Figure 2. (a) DLTS spectra from 200 K to 350 K. (b) Arrhenius plot of E1. (c) N_T (trap concentration) and N_{Ta} (lambda-corrected trap concentration) as a function of depletion region width under U_R (w_R).

was narrower than the thickness of homogeneous epilayer (11 μm). Therefore, E1 is considered to be located in the homogeneous epilayer.

Accurate extraction of trap concentration plays a crucial role in identifying the origins and providing feedback for optimization of growth conditions [23]. Figure 2(c) depicts the trap concentration N_T extracted from equation (3) as a function of depletion width w_R, which can be controlled by changing U_R [24]:

$$N_T = 2\frac{\Delta C_R}{C_R}N_s \tag{3}$$

where ΔC_R and C_R represent the capacitance transient amplitude and capacitance under U_R, respectively. It was

observed that the N_T was enhanced with increasing w_R. The phenomenon of N_T varying with the depletion region width is related to the fact that the traps near the edge of depletion region do not emit carriers, also known as lambda effect [25]. Failure to take lambda effect into account would lead to an underestimated N_T than the actual value. Considering lambda effect, the lambda-corrected trap concentration (N_{Ta}) in the device could be accurately determined by equation (4) [24] (More details about lambda-corrected trap concentration can be found in the supplementary material):

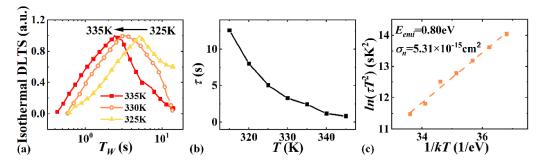$$N_T = N_{\text{Ta}}\left(1 - \frac{\lambda}{w_R}\right)^2 \tag{4}$$

Figure 3. (a) Isothermal DLTS from 325 K to 335 K. (b) T-dependent τ extracted from isothermal DLTS. (c) Arrhenius plot of E1.

where λ denotes non-emission region width and could be obtained by exploration of depletion width dependent carrier concentration. In this study, N_{Ta} and λ were extracted to be 2.48×10^{13} cm^{-3} and 267.78 nm, respectively.

Figure 3(a) shows the normalized isothermal DLTS of E1 as a function of measurement time (T_W) from 325 K to 335 K (reverse bias $U_R = -20$ V, filling pulse $U_P = -0.5$ V and filling pulse width $t_P = 0.8$ s). The emission time constants (τ) were extracted from the peak location of isothermal DLTS spectra at each temperature step. As heating the sample up, the signal peak of E1 exhibits shorter emission time constants. The extracted emission time constants of E1 at different temperatures are summarized in figure 3(b). When the temperature increased from 315 K to 345 K, the emission time constant of E1 steadily reduced from 12.56 s to 0.81 s, indicating an accelerated emission process at higher temperature.

As shown in figure 3(c), the T-dependent relationship can be fitted by Arrhenius relation, which is expressed as following equation [4]:

$$\ln\left(\tau T^2\right) = \frac{E_{\text{emi}}}{kT} - \ln(\gamma \sigma_{\text{n}}) \tag{5}$$

where γ is a constant value corresponding to effective electron mass m_{e}^*. The fitting reveals an activation energy for emission E_{emi} of 0.80 eV and capture cross section σ_{n} of 5.31×10^{-15} cm^2, which matches well with the trap properties from DLTS in figure 2(b).

Figure 4(a) shows electric-field-dependent (E-dependent) emission time constant (τ) extracted from isothermal DLTS at four temperature steps from 320 K to 335 K. Assuming that the N_{s} in the entire depletion region is uniform, maximum electric field can be considered as representative of electric field to investigate the electric-field-enhanced emission process [26]. The local electric field ($E(x)$) can be obtained from V_{bi} and N_{s} [17]:

$$E(x) = \sqrt{\frac{2qN_{\text{s}}(V_{\text{bi}} - U_{\text{R}})}{\varepsilon_{\text{r}}\varepsilon_0} - \frac{qN_{\text{d}}}{\varepsilon_{\text{r}}\varepsilon_0}x} \tag{6}$$

where x is the distance to the metal-semiconductor interface. To characterize the emission time constant, the average electric field in the depletion region from $w_P - \lambda$ to $w_R - \lambda$ is used, where w_P and w_R are the depletion region width under U_P and U_R, respectively.

The emission time constant was measured with reverse bias U_R varying from -1 V to -50 V, and corresponding average electric field changed from 1.06×10^5 V cm^{-1} to 3.37×10^5 V cm^{-1}. When the electric field applied on the device was relatively low (Region I in figure 4(a)), τ decreased significantly as increasing electric field, indicating that the emission process can also be accelerated by elevating electric field. In this region, $\ln(e_{\text{n}})$ is found to be linearly proportional to E^2 from 320 K to 335 K, as shown in figure 4(b). The dependence between $\ln(e_{\text{n}})$ and E^2 suggests that the emission mechanism of E1 could be well modeled by phonon-assisted tunneling (PAT), as described by equation (7) [27]:

$$\ln\left(e_{\text{n}}\right) = \frac{2\pi q^2 \tau_{\text{PAT}}^3 E^2}{3m_{\text{e}}^* h} + \ln\left(\frac{1}{\tau_0}\right) \tag{7}$$

where τ_{PAT} is the tunneling time of PAT and τ_0 is the emission time constant at zero-field strength. The first term of equation (7) is linearly dependent on E^2, and second term is independent of E. With increasing the electric field, the absolute value of first item in equation (7) become comparable with the absolute value of second item, indicating an electric-field-enhanced emission process. This process can be interpreted by the lowering and thinning of potential barrier due to the strengthened electric field [27, 28]. Figure 4(c) summarizes extracted τ_0 at different temperatures. The T-dependent τ_0 reveals the influence of temperature on the emission process at zero electric field. When the temperature increases from 320 K to 335 K, it is observed that the τ_0 decreases from 17.94 s to 4.73 s, indicating a temperature-enhanced emission process at zero electric field. As a specific emission time constant, τ_0 has the relationship with temperature as well:

$$\ln\left(\tau_0 T^2\right) = \frac{E_{\text{emi0}}}{kT} - \ln(\gamma \sigma_{\text{n}}) \tag{8}$$

where E_{emi0} is the activation energy for emission at zero-field strength. Figure 4(d) exhibits the Arrhenius plot at zero-field strength, with the result of $E_{\text{emi0}} = 0.87$ eV and $\sigma_{\text{n}} = 6.86 \times 10^{-15}$ cm^{-2}. E_{emi0} is slightly larger than E_{emi} due to the difference of electric field. An increasing of electric field will contribute to the lower or thinner potential barrier for emission [17, 28], as a result, E_{emi0} under zero-field strength should be slightly larger than E_{emi}. The τ_{PAT} is extracted to determine the duration for the carriers to tunnel through the barrier between the trap and the conduction band minimum
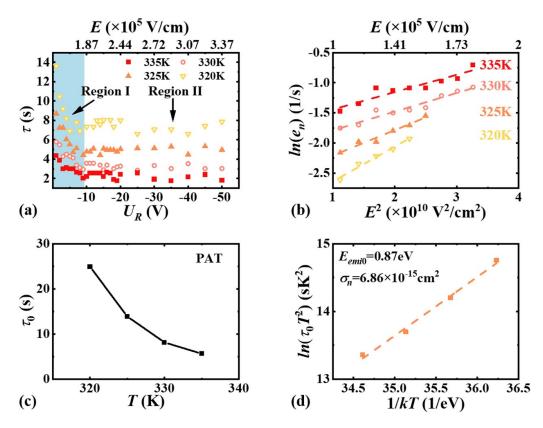
Figure 4. (a) Electric-field-dependent τ extracted from isothermal DLTS from 320 K to 335 K. (b) The emission rate (e_n) of E1 from 320 K to 335 K. (c) τ_0 from 320 K to 335 K. (d) Arrhenius plot of E1 at zero-field strength.

with the assistance of phonons. For the same temperature range, the τ_{PAT} slightly decreases from 19.11 fs to 14.92 fs. As a part of the emission process, τ_{PAT} will be accelerated by the temperature as τ. When the electric field applied on the device was further enhanced (Region II in figure 4(a), $E \geqslant 1.81 \times 10^5$ V cm^{-1} at 330 K), the emission time constant was slightly shortened, which is observed in other studies as well [29, 30]. The emission mechanism in Region II is regarded to be direct tunneling (DT) without the assistance of phonons. Compared to PAT, DT needs a relatively larger electric field to trigger, and once triggered further enhanced electric field have little influence on the emission process [31]. The critical electric field to distinguish Region I and II in figure 4(a) raises with increased temperature, which also confirmed that DT was the mechanism for relatively high electric field.

As shown in figure 5, capacitance transient signal was utilized to investigate the capture process of E1. Figure 5(a) illustrates the ratio of capacitance transient signal amplitude as a function of the temperature with different filling pulse widths t_P. ΔC is the capacitance transient amplitude which reveals the number of traps being filled, and ΔC_{max} represents the capacitance transient amplitude when traps are completely filled with a long t_P, which was set to be 10 ms in this study. When t_P was set to 1 ms, the ratio of capacitance transient amplitude was close to 100% for different temperature steps, indicating that a filling time of 1 ms was long enough to fill all the traps, and the capture time constant was less than 1 ms. With a fixed t_P of 0.01 ms, the capacitance transient amplitude ratio was

enhanced from 89% to 98% as increasing temperature from 315 K to 345 K, inferring that higher temperature could accelerate the capture process as well.

Figure 5(b) displays extracted capture barrier energy E_{cap} by the following equation [32]:

$$\ln(f) = -\frac{E_{cap}}{kT} + \ln(H) \tag{9}$$

where H is a constant which is independent of temperature, and f is a function related to ΔC and temperature [32]:

$$f = \frac{\ln\left(1 - \frac{\Delta C(t_p)}{\Delta C_{max}}\right)}{\sqrt{T}}. \tag{10}$$

An E_{cap} of 0.15 eV is extracted from the slope of linear fitting in Arrhenius plot, smaller than the E_{emi}. The lower E_{cap} suggests that less energy is required to capture electrons in the capture process compared with the emission process.

Figure 5(c) depicts the physical relationship between E_{emi} and E_{cap}, and two parabolas display the total energy in different conditions. The black solid parabola shows the circumstance when the electron is not captured by E1, and the orange dashed one represents the situation when E1 captures the electron. During the capture process, the electron needs to overcome the energy barrier from the valley of the black solid parabola to the intersection, called E_{cap}. Meanwhile, E_{emi} refers to the activation energy for emission as well.
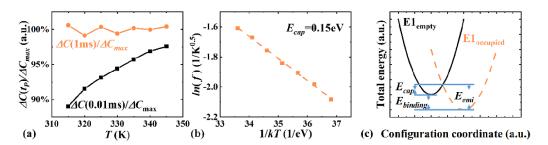
Figure 5. (a) Capacitance transient signal amplitude ratio of different t_P. (b) Arrhenius plot of E1 to extract E_{cap}. (c) The configuration coordinate diagram for the total energy before (black solid line) and after (orange dashed line) capture process.

Table 1. Comparison of trap properties between E1 and other similar traps in references. (NA means not applicable in the table.).

β-Ga$_2$O$_3$ Structure	Doping element	E_{emi} (eV)	σ_n (cm^2)	N_T (cm^{-3})	Emission mechanism	E_{cap} (eV)
Epilayer [This work]	Si	0.80	6.40×10^{-15}	2.48×10^{13} (N_{Ta})	PAT, DT	0.15
Bulk material [6]	undoped	0.78	7×10^{-15}	$\sim 10^{16}$	NA	NA
Epilayer [6]	NA	0.78	NA	$\sim 6 \times 10^{13}$	NA	NA
Bulk material [16]	Sn	0.80	10^{-15}–10^{-14}	NA	PAT	NA
Proton irradiated epilayer [12]	Si	0.75	6.5×10^{-15}	3.2×10^{14} (N_{Ta})	NA	0.36

As shown in figure 5(c), E_{emi} extracted from DLTS consists of two constituent parts, the capture barrier energy E_{cap} and the binding energy $E_{binding}$ [19, 33]:

$$E_{emi} = E_{cap} + E_{binding}. \tag{11}$$

E_{cap} and $E_{binding}$ reveal the requisite energy for electrons to be captured by traps and the depth of E1 with respect to the conduction band minimum, respectively. Therefore, $E_{binding}$ of E1 was determined to be 0.65 eV.

Table 1 summarizes the trap characteristics in this study and in the literatures. The trap concentration of E1 is 2.48×10^{13} cm^{-3}, comparable with the result in an β-Ga$_2$O$_3$ SBD with epilayer ($\sim 6 \times 10^{13}$ cm^{-3}) [6], but much smaller than the result in an undoped β-Ga$_2$O$_3$ SBD without epilayer ($\sim 10^{16}$ cm^{-3}) [6]. Therefore, it can be concluded that a high-quality epilayer may have a lower trap concentration, which is also declared by Polyakov *et al* [12]. PAT has been successfully applied to model the emission mechanism of both trap in Sn-doped n-type β-Ga$_2$O$_3$ substrate [16] and the single trap in Si-doped epilayer. This work also revealed another emission mechanism: DT in Region II ($E \geqslant 1.81 \times 10^5$ V cm^{-1} at 330 K). With the investigation of T-dependent capture process, E_{cap} of 0.15 eV was extracted in this study, smaller than 0.36 eV in proton irradiated Si-doped β-Ga$_2$O$_3$ layer [12], indicating that proton irradiation may enhance the capture barrier.

4. Conclusion

In summary, temperature-dependent electrical characteristics of vertical β-Ga$_2$O$_3$ SBD were analyzed from 200 K to 350 K. A deep level trap E1 (E_{emi} = 0.80 eV) in the homogeneous epilayer was investigated using DLTS. By isothermal DLTS, the lambda-corrected trap concentration and non-emission

region width are determined to be 2.48×10^{13} cm^{-3} and 267.78 nm, respectively. From 315 K to 345 K, emission time constant declines from 12.56 s to 0.81 s, revealing emission process can be accelerated by increasing temperature. The electric-field-enhanced trap emission kinetics were studied in addition to the impact of temperature. Two regions in electric-field-dependent emission process are observed. When $E \leqslant 1.81 \times 10^5$ V cm^{-1} at 330 K, the emission time of E1 is considered to comply with PAT, whereas DT was employed to explain the emission process when an enhanced electric field is applied ($E \geqslant 1.81 \times 10^5$ V cm^{-1} at 330 K). Through analysis of capacitance transient signal, thermal-enhanced capture process has been quantitatively studied, and capture barrier energy of 0.15 eV was extracted.

Data availability statement

The data that support the findings of this study are available upon reasonable request from the authors.

Acknowledgments

ORCID iDs

Haolan Qu https://orcid.org/0000-0002-2907-6565
Jiaxiang Chen https://orcid.org/0000-0001-6793-4025
Yu Zhang https://orcid.org/0000-0002-5017-6771

Xing Lu [ORCID] https://orcid.org/0000-0001-5808-9552
Xinbo Zou [ORCID] https://orcid.org/0000-0002-9031-8519

References

[1] Wang Z, Chen X, Ren F-F, Gu S and Ye J 2021 *J. Phys. D: Appl. Phys.* **54** 043002

[2] Higashiwaki M, Sasaki K, Murakami H, Kumagai Y, Koukitu A, Kuramata A, Masui T and Yamakoshi S 2016 *Semicond. Sci. Technol.* **31** 034001

[3] Chabak K D *et al* 2019 *Semicond. Sci. Technol.* **35** 013002

[4] Chen J, Luo H, Qu H, Zhu M, Guo H, Chen B, Lv Y, Lu X and Zou X 2021 *Semicond. Sci. Technol.* **36** 055015

[5] Fares C, Ren F and Pearton S J 2018 *ECS J. Solid State Sci. Technol.* **8** Q3007–12

[6] Ingebrigtsen M E, Varley J B, Kuznetsov A Y, Svensson B G, Alfieri G, Mihaila A, Badstübner U and Vines L 2018 *Appl. Phys. Lett.* **112** 042104

[7] Farzana E, Mauze A, Varley J B, Blue T E, Speck J S, Arehart A R and Ringel S A 2019 *APL Mater.* **7** 121102

[8] Hao S J *et al* 2019 *J. Appl. Phys.* **125** 105701

[9] Sasaki K, Kuramata A, Masui T, Víllora EG, Shimamura K and Yamakoshi S 2012 *Appl. Phys. Express* **5** 035502

[10] Murakami H *et al* 2014 *Appl. Phys. Express* **8** 015503

[11] Yang J, Ren F, Tadjer M, Pearton S J and Kuramata A 2018 *ECS J. Solid State Sci. Technol.* **7** Q92–Q6

[12] Polyakov A, Smirnov N, Schemerov I, Yakimov E, Yang J, Ren F, Yang G, Kim J, Kuramata A and Pearton S 2018 *Appl. Phys. Lett.* **112** 032107

[13] McGlone J F, Xia Z, Joishi C, Lodha S, Rajan S, Ringel S and Arehart A R 2019 *Appl. Phys. Lett.* **115** 153501

[14] Polyakov A Y, Smirnov N B, Shchemerov I V, Gogova D, Tarelkin S A and Pearton S J 2018 *J. Appl. Phys.* **123** 115702

[15] Wang B, Look D and Leedy K 2019 *J. Appl. Phys.* **125** 105103

[16] Polyakov A Y, Lee I-H, Smirnov N B, Shchemerov I V, Vasilev A A, Chernykh A V and Pearton S J 2020 *J. Phys. D: Appl. Phys.* **53** 304001

[17] Sun R, Ooi Y K, Bhattacharyya A, Saleh M, Krishnamoorthy S, Lynn K G and Scarpulla M A 2020 *Appl. Phys. Lett.* **117** 212104

[18] Craven R A and Finn D 1979 *J. Appl. Phys.* **50** 6334–43

[19] Hacke P, Detchprohm T, Hiramatsu K, Sawaki N, Tadatomo K and Miyake K 1994 *J. Appl. Phys.* **76** 304–9

[20] Higashiwaki M *et al* 2016 *Appl. Phys. Lett.* **108** 133503

[21] Chen J, Zhu M, Lu X and Zou X 2020 *Appl. Phys. Lett.* **116** 062102

[22] Lang D V 1974 *J. Appl. Phys.* **45** 3023–32

[23] Kanegae K, Narita T, Tomita K, Kachi T, Horita M, Kimoto T and Suda J 2020 *Jpn. J. Appl. Phys.* **59** SGGD05

[24] Kanegae K, Horita M, Kimoto T and Suda J 2018 *Appl. Phys. Express* **11** 071002

[25] Zohta Y and Watanabe M O 1982 *J. Appl. Phys.* **53** 1809–11

[26] Hu Z *et al* 2019 *Nanoscale Res. Lett.* **14** 2

[27] Ganichev S D, Ziemann E, Prettl W, Yassievich I N, Istratov A A and Weber E R 2000 *Phys. Rev.* B **61** 10361–5

[28] Katzenmeyer A M, Léonard F, Talin A A, Wong P-S and Huffaker D L 2010 *Nano Lett.* **10** 4935–8

[29] Danno K, Kimoto T and Matsunami H 2005 *Appl. Phys. Lett.* **86** 122104

[30] Lang M, Pensl G, Gebhard M, Achtziger N and Uhrmacher M 1991 *Appl. Phys.* A **53** 95–101

[31] Ganichev S D, Prettl W and Yassievich I N 1997 *Phys. Solid State* **39** 1703–26

[32] Criado J, Gomez A, Calleja E and Muñoz E 1988 *Appl. Phys. Lett.* **52** 660–1

[33] Huang Q, Grimmeiss H G and Samuelson L 1985 *J. Appl. Phys.* **58** 3068–71